Journal of Chromatography B 1141 (2020) 122022

Contents lists available at ScienceDirect

Journal of Chromatography B

journal homepage: www.elsevier.com/locate/jchromb

Lipid alterations in the skeletal muscle tissues of mice after weight regain by feeding a high-fat diet using nanoflow ultrahigh performance liquid chromatography-tandem mass spectrometry

Jung Yong Eum[a], Gwang Bin Lee[a], Sun Shin Yi[b,c], Il Yong Kim[c,d], Je Kyung Seong[c,d,*], Myeong Hee Moon[a,*]

[a] Department of Chemistry, Yonsei University, Seoul 03722, Republic of Korea
[b] Department of Biomedical Laboratory Science, College of Biomedical Sciences, Soonchunhyang University, Asan, Republic of Korea
[c] Korea Mouse Phenotyping Center, Seoul National University, Seoul, Republic of Korea
[d] Laboratory of Developmental Biology and Genomics, Research Institute for Veterinary Science, and BK21 Program for Creative Veterinary Science, College of Veterinary Medicine, Interdisciplinary Program for Bioinformatics, and BIO-MAX Institute, Seoul National University, Seoul, Republic of Korea

ARTICLE INFO

Keywords:
High-fat diet
Weight regain
Skeletal muscle tissues
Lipidomics
Mouse
nUHPLC-ESI-MS/MS

ABSTRACT

This study investigated lipid alterations in muscle tissues [gastrocnemius (Gas) and soleus (Sol)] of mice under different diet programs (weight gain, weight maintenance, weight regain, and controls) by nanoflow ultrahigh pressure liquid chromatography-electrospray ionization-tandem mass spectrometry. Since overloaded lipids in the skeletal muscle tissues by excessive fat accumulation are related to insulin resistance leading to type II diabetes mellitus, analysis of lipid alteration in muscle tissues with respect to high-fat diet (HFD) is important to understand obesity related diseases. A total of 345 individual lipid species were identified with their molecular structures, and 184 lipids were quantified by selected reaction monitoring method. Most triacylglycerol (TG) and phosphatidylethanolamine (PE) species displayed a significant (> 2-fold, $p < 0.01$) increase in both the Gas and Sol and to a larger degree in the Gas. However, lipid classes involved in insulin resistance and anti-inflammatory response, including lysophosphatidylcholine (18:0), diacylglycerol (16:0_18:1, 16:0_18:2, and 18:1_18:1), ceramide (d18:1/24:0 and d18:1/24:1), and phosphatidylinositol (18:0/20:4), showed a significant accumulation in the Sol exclusively after HFD treatment. In addition, the lipid profiles were not significantly altered in mice that were fed HFD only for the last 4 weeks (weight gain group), suggesting that consuming HFD in the younger age period can be more effective in the Gas. This study reveals that lipid classes related to insulin resistance accumulated more in the Sol than in the Gas following HFD treatment and the weight regain program perturbed lipid profiles of the Sol to a greater extent than that by the other diet programs, confirming that the Sol tissue is more influenced by HFD than Gas.

1. Introduction

The prevalence of overweight [body mass index (BMI) of 25–29.9 kg/m^2] and obesity (BMI ≥ 30 kg/m^2) has rapidly increased worldwide and is a global public health concern. Excessive body fat accumulation due to high-fat diet (HFD) is the major contributor to obesity, leading to insulin resistance that further increases the risk of cardiovascular diseases and type II diabetes mellitus (T2DM) [1]. Among the liver, adipose tissue, and skeletal muscles, lipid accumulation in the skeletal muscle has been associated with the insulin resistance [2,3]. Lipids are not only the major components of the cell wall but also important sources of energy reserves and mediators in signal

Abbreviations: BMI, body mass index; Cer, ceramide; CID, collision-induced dissociation; DG, diacylglycerol; ESI, electrospray ionization; HexCer, monohexosylceramide; HFD, high-fat diet; Gas, Gastrocnemius; LOD, limit of detection; LOQ, limit of quantitation; LPA, lysophosphatidic acid; LPC, lysophosphatidylcholine; LPE, lysophosphatidylethanolamine; LPG, lysophosphatidylglycerol; LPI, lysophosphatidylinositol; LPS, lysophosphatidylserine; MS, mass spectrometry; PA, phosphatidic acid; PC, phosphatidylcholine; PCA, principal component analysis; PCp, PC plasmalogen; PE, phosphatidylethanolamine; PEp, PE plasmalogen; PG, phosphatidylglycerol; PI, phosphatidylinositol; PS, phosphatidylserine; SM, sphingomyelin; SRM, selected reaction monitoring; Sol, Soleus; TG, triacylglycerol; ZDF, Zucker diabetic fatty; UHPLC, ultrahigh-performance liquid chromatography

* Corresponding authors at: Korea Mouse Phenotyping Center, Seoul National University, Seoul, Republic of Korea (J.K. Seong).
E-mail addresses: snumouse@snu.ac.kr (J.K. Seong), mhmoon@yonsei.ac.kr (M.H. Moon).

https://doi.org/10.1016/j.jchromb.2020.122022
Received 13 November 2019; Received in revised form 10 January 2020; Accepted 6 February 2020
Available online 07 February 2020
1570-0232/

transduction between cells and are involved in cell proliferation and apoptosis [4,5]. Lipid accumulation in skeletal muscles has been studied to elucidate the relationship between lipid profiles and insulin resistance. Among the various classes of lipids, triacylglycerol (TG), diacylglycerol (DG), and ceramides (Cer) are reported to be associated with the incidence of insulin resistance [6–9]. Several studies have revealed that excess accumulation of intramuscular TG is associated with insulin resistance in human [10,11] and animal models [12]. However, insulin sensitivity is markedly maintained in the skeletal muscles of trained endurance athletes despite the accumulation of intramuscular TG [13,14]. This could be owing to the enhanced lipid oxidation capacity in trained athletes due to increased number of mitochondria. Other studies have shown insulin sensitivity to be associated with specific TGs with saturated acyl chains compared to the total serum TG levels [15] and accumulation of DG in the muscle and liver [16–18].

Obesity and T2DM are related to the type of muscle fiber, reduction in the number of mitochondria, and their associated dysfunction [19]. Muscle fibers are grouped into three major categories: type I (oxidative slow-twitch), type IIa (oxidative fast-twitch), and type IIb (glycolytic fast-twitch) depending on the energy production mechanism in the cell [20]. HFD induces pre-diabetes in young mice with mitochondrial dysfunction and leads to a shift in the skeletal muscles from oxidative to glycolytic type [21–24]. Studies have shown that mitochondrial density and lipid content were higher in the soleus (Sol), a slow-twitch type I oxidative skeletal muscle, than in the gastrocnemius (Gas), a fast-twitch glycolytic muscle [25,26]. Excessive accumulation of lipids in glycolytic muscle can be a major contributor toward insulin resistance due to the increased activity of enzymes interfering with insulin signaling [27]. A recent study showed that several DG and TG species accumulated (> 2–3 times) in both the Gas and Sol of Zucker diabetic fatty (ZDF) rats [28]. Nevertheless, these lipids were significantly reduced in the Sol but not in the Gas after treadmill exercise, suggesting that physical exercise effectively lowers the accumulated DG and TG only in the oxidative slow-twitch fibers. The relationship between HFD and muscle type has not been widely discussed. Studies indicate that weight regain after reduced obesity in human and animal models led to fat gain, which enhanced adipose tissue inflammation and impaired systemic glucose tolerance [29,30]. However, the mechanisms involved in metabolic dysfunction induced by weight regain are not fully understood.

In the present study, we investigated the effect of HFD on the lipid profiles of mouse skeletal muscles at the molecular level by using nanoflow ultrahigh performance liquid chromatography (LC) with tandem mass spectrometry (nUHPLC-ESI-MS/MS). Recent advances in LC-MS facilitated the simultaneous separation and structural determination of several hundreds of lipids from plasma/serum, urine, and tissue samples [31–35] and lipid analysis can be achieved at a high speed (< 20 min) by employing nUHPLC-ESI-MS/MS [36,37]. Lipid extracts from the Sol and Gas were systematically examined with variations in diet programs, namely, weight gain, weight maintenance, weight regain, and normal diet. Lipid analysis was accomplished by non-targeted identification of molecular structures based on data-dependent collision-induced dissociation experiments during nUHPLC-ESI-MS/MS, followed by selected reaction monitoring (SRM)-based targeted quantification of individual lipid samples. With statistical evaluation, lipid species showing significant changes in comparison with the respective control groups were screened for characteristic lipid species for weight gain, weight maintenance, and weight regain.

2. Materials and methods

2.1. Chemicals and reagents

A total of 19 lipid standards were used for nUHPLC optimization and for quantification standards: lysophosphatidylcholine (LPC) 16:0, phosphatidylcholine (PC) 12:0/12:0, PC plasmalogen (PCp) P-18:0/22:6, lysophosphatidylethanolamine (LPE) 18:0, phosphatidylethanolamine (PE) 16:0/16:0, PE plasmalogen (PEp) P-18:0/18:1, phosphatidic acid (PA) 12:0/12:0, lysophosphatidylglycerol (LPG) 18:0, phosphatidylglycerol (PG) 18:0/18:0, lysophosphatidylinositol (LPI) 20:4, phosphatidylinositol (PI) 18:0/20:4, lysophosphatidylserine (LPS) 16:0, phosphatidylserine (PS) 12:0/12:0, diacylglycerol (DG) 16:0/18:1, triacylglycerol (TG) 18:0/18:0/18:1, sphingomyelin (SM) d18:1/16:0, ceramide (Cer) d18:1/14:0, Cer d18:1/22:0, monohexosylceramide (HexCer) d18:1/12:0. In addition, 14 lipid standards with odd-numbered fatty acyl chain were used as internal standards for quantification: LPC 17:0, PC 13:0/13:0, LPE 17:1, PE 17:0/17:0, LPG 17:1, PG 15:0/15:0, LPI 17:1, PI 12:0/13:0, PS 17:0/17:0, D_5-DG 17:0/17:0, D_5-TG 17:0/17:1/17:0, SM d18:1/17:0, Cer d18:1/17:0, HexCer d18:1/17:0. All lipid standards were purchased from Matreya, LLC. (Pleasant Gap, PA, USA) and Avanti Polar Lipids, Inc. (Alabaster, AL, USA). HPLC grade solvents (water, acetonitrile, methanol, and isopropanol) and methyl-*tert*-butyl ether (MTBE) were purchased from Avantor Performance Materials (Center Valley, PA, USA). Ammonium hydroxide and ammonium formate were purchased from Sigma-Aldrich (St. Louis, MO, USA). For column preparation, fused silica capillary tubes and plumbing supplies were procured from Polymicro Technology, LLC. (Phoenix, AZ, USA). Packing materials for preparing analytical columns were Watchers® ODS-P C-18 particles (3 μm and 100 Å) from Isu Industry Corp. (Seoul, Korea) and 1.7 μm ethylene bridged hybrid (BEH) particles unpacked from ACQUITY UPLC® BEH C18 column (2.1 mm × 100 mm) of Waters™ (Milford, MA, USA). A PEEK microcross was purchased from IDEX Health & Science, Oak Harbor, WA, USA).

2.2. Animals

Thirty-six male mice (C57BL6/N) from Central Lab. Animal Inc. (Seoul, Korea) were used for this study. Mice at 5 weeks of age were transferred to the animal facility at Korea Mouse Phenotyping Center (KMPC), Seoul National University. Mice were fed with a normal diet (NIH-31, chow diet from Zeigler Bros, Inc., Gardners, PA, USA) *ad libitum* and tap water, before the dietary experiments began. Mice were maintained under 24 ± 2 ˚C with a 12 h light/dark cycle. For HFD, 60% kcal% fat (#D12492, Research Diets, NJ, USA) were provided to the mice. For the first 8 weeks after relocation, half the mice (n = 18) were fed with a normal diet and the other half with HFD. At the end of 8 weeks, 6 animals in each group were sacrificed and classified as N (control) and F (weight gain). The remaining 12 animals in both groups were fed with normal diet for 4 weeks and then further divided into two subgroups to be fed with either normal or HF diet for another 4 weeks. The resulting 4 subgroups were NNN (control), FNN (weight maintenance), NNF (weight gain), and FNF (weight regain) as shown in Scheme 1 (n = 6).

The two types of skeletal tissue samples (Gas and Sol) were obtained from 6 mice in each dietary group. The mice were killed by exposure to CO_2. Animal experiments followed the 'Guide for Animal Experiments,' edited by Korean Academy of Medical Sciences, and were approved by

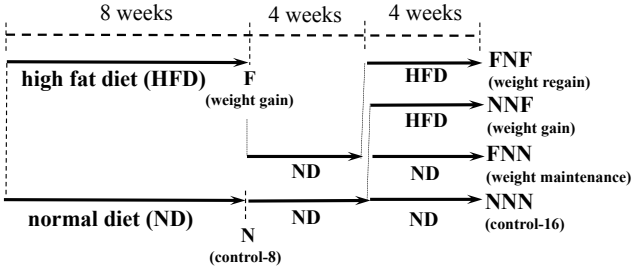

Scheme 1. Dietary stages of 6 different mouse groups.

the Institutional Animal Care and Use Committee (IACUC) of Seoul National University (Permit Number: SNU-140205-2-1). Before extracting tissues, all mice were perfused after anesthesia for sample quality control. Changes in body weights and blood glucose and total cholesterol levels along with details of the histopathological examination of liver tissue are provided in Lee et al. [38].

2.3. Lipid extraction

A total of 72 samples were lyophilized into fine powder. For lipid identification purposes, the same portion of the tissue sample from each animal was pooled together in each group (n = 6), and 4 mg was used for lipid extraction. For targeted lipid quantification, 4 mg of each animal sample was used. The pooled or individual tissue sample was suspended in 150 μL of a 9:1 (v/v) mixture of H_2O and phosphate-buffered saline and subjected to tip-sonication for 1 min in an ice bath. After sonication, 300 μL CH_3OH was added to the sonicated mixture in the ice bath and vortexed for 10 min. Lipids were extracted following a two-stage extraction method using MTBE/CH_3OH [39]. The resulting mixture was added with 1 mL MTBE and 100 μL MS-grade H_2O, vortexed for 1 h, and centrifuged at 1000 × g for 10 min. Then the upper organic layer was transferred to a new tube and the remaining aqueous layer was mixed with 400 μL CH_3OH for secondary extraction followed by centrifugation at 1000*g* for 10 min. The resulting organic layer was taken out to merge with the previously collected organic layer. Organic solvents in lipid solution were evaporated by vacuum centrifuge for 3 h. Dried lipid extracts were re-constituted at a concentration of 10 μg/μL with $CHCl_3$:CH_3OH (1:9, v/v), and then stored at −80 °C. For nUHPLC-ESI-MS/MS analysis, frozen lipid extract was diluted to a concentration of 2 μg/μL with (9:1, v/v) CH_3OH:H_2O. Extraction efficiency of lipids was measured by calculating the recovery value of 14 lipid standards (1 pmol each) spiked before and after lipid extraction of Gas tissue based on nUHPLC-ESI-MS/MS. The recovery values were within 82.3–106.5% for all 14 standard lipids and the detailed data were added to Table S1 of Supplementary data.

2.4. nUHPLC-ESI-MS/MS analysis of lipids

For the identification and quantification of muscle lipids, two sets of nUHPLC-ESI-MS/MS instruments were used: a Dionex Ultimate 3000 RSLCnano System with LTQ Velos ion trap MS from Thermo Fisher Scientific™ (San Jose, CA, USA) for non-targeted lipid identification and a nanoACQUITY UPLC system from Waters™ coupled with a TSQ Vantage triple-stage quadrupole MS from Thermo Fisher Scientific™ for targeted quantification. The pulled-tip capillary column was prepared in the laboratory by pulling one end of a fused silica capillary (100 μm of inner diameter (ID), 360 μm of outer diameter) with flame to make a sharp needle. The column tip (0.5-cm portion) was packed with 3 μm–100 Å Watchers® ODS-P C18 particles from Isu Industry Corp. (Seoul, Korea) to prepare self-assembled frit under N_2 gas (1000 psi) and the rest of column (6.5-cm long) was packed with 1.7 μm BEH particles which was unpacked from a Waters™ ACQUITY UPLC® BEH C18 column. The analytical column was connected to nUHPLC pump using a capillary tube (50 μm ID) via a PEEK micro-cross from IDEX Health & Science (Oak Harbor, WA, USA) of which the other two ports were connected with a Pt wire for ESI voltage supply and a pressure capillary (20 μm ID) leading to on/off switching valve for splitting pump flow.

For gradient elution, both nUHPLC-ESI-MS/MS systems use the same set of mobile phases for binary gradient elution: H_2O:CH_3CN (9:1, v/v) for mobile phase A and CH_3OH:CH_3CN:IPA (2:2:6, v/v) for mobile phase B, added with a mixture of ionization modifiers (0.05% NH_4OH and 5 mM NH_4HCO_2) to be used in both positive and negative ion modes. For non-targeted identification of muscular lipids with molecular structures, 3 μg of the lipid extract from each pooled sample was utilized for each nUPLC-ESI-MS/MS analysis. Sample loading to the analytical column was made via autosampler with the mobile phase A for 7.5 min at a flow rate of 1.0 μL/min with the switching valve off. After completing the sample loading, the pump flow rate was increased to 12 μL/min with the switching valve on so that the final flow rate to the analytical column was adjusted to 300 nL/min. The gradient elution began by ramping mobile phase B from 60% to 80% for 7.5 min, further to 100% for 20 min, and maintained at 100% for 8 min. Then, it was resumed to 0% and maintained for 5 min to re-equilibrate the column. The *m/z* range of precursor MS scan was set to 300–1000 amu with 3.0 kV of ESI voltage for both positive and negative ion modes. For data-dependent collision induced dissociation (CID) experiments, 40% normalized collision energy was applied. The molecular structure of lipid was determined from the fragment ion spectra using LiPilot, a PC-based software developed in our laboratory [40].

For targeted quantification, lipid extract from each animal was analyzed with the addition of 14 different internal standards (1 pmol of each IS) in Table S2. For each sample, 3 μg of lipid extracts were loaded to the same analytical column utilized in the non-targeted identification. Sample loading was made with the mobile phase A at 0.8 μL/min for 8 min. The pump flow rate during the gradient elution was 17 μL/min which was to reduce the dwell time and the column flow rate was adjusted to 300 nL/min using the switching valve likewise. Gradient elution began with 60% B and was increased to 85% B for 10 min, further to 100% for 15 min, and maintained for 5 min. Then it was resumed to 0% B for re-equilibration. Lipid quantification was made for the identified lipid species using selected reaction monitoring (SRM) method in which precursor ion and one of its fragments as a quantifier ion were scanned by the triple-stage quadrupole MS system. Types of precursor ions and quantifier ions for each lipid class with the collision energies specific to lipid class are listed in Table S2. For rapid SRM quantification, each lipid species was programmed for 2-min time interval (retention time ± 1 min) for detection instead of scanning all identified lipids simultaneously. SRM quantification was made in the polarity switching mode which detects ions at positive and negative ion mode alternatively: LPC, PC, LPE, PE, DG, TG, SM, Cer, and HexCer in positive ion mode, and LPG, PG, LPI, PI, PS in negative ion mode. Collision energy was differently assigned by lipid classes (Table S2): 20 V for LPE and PE; 30 V for DG and TG; 35 V for PS; 40 V for LPC, PC, PEp, LPG, PG, LPI, SM, Cer, and HexCer; 45 V for PI.

Limit of detection (LOD) and limit of quantitation (LOQ) for 14 lipid classes were calculated from the calibration curve of each IS spiked to the lipid extract of each tissue by varying concentration of the IS and listed in Table S3. Briefly, LOD/LOQ values ranged from 0.0021/0.070 pmol (TG 17:0/17:1/17:0 D_5) to 0.096/0.318 pmol (SM d18:1/17:0) in Gas. Lipid species below the LOQ in each lipid class was removed from the quantified data lists. The quantified amount of each lipid was reported by the corrected peak area, the ratio of peak area of an individual lipid species in comparison with that of the class-specific IS, which is a good estimate of the pmol amount of each species assuming that the polar head group is more significant factor than the length of the acyl chain and the degree of unsaturation in this level [41,42]. Data analysis was carried out with SPSS software (version 20.0, IBM corp., Armonk, NY, USA) for Student's *t*-test and Minitab 17 (http://www.minitab.com) for principal component analysis (PCA).

3. Results

3.1. Identification and SRM quantification of muscle lipids

Non-targeted identification of muscle lipids was carried out by nUHPLC-ESI-MS/MS at conditions optimized using lipid standards shown in base peak chromatograms (BPCs) (Fig. S1). Relative standard deviations of average retention time and peak width were 0.4 ± 0.3% and 16.6 ± 6.7 s, respectively. BPCs of lipid extracts from the Gas and Sol of both NNN and FNF groups are shown in Fig. S2. A total of 345 lipids were identified with their molecular structures, of which 184

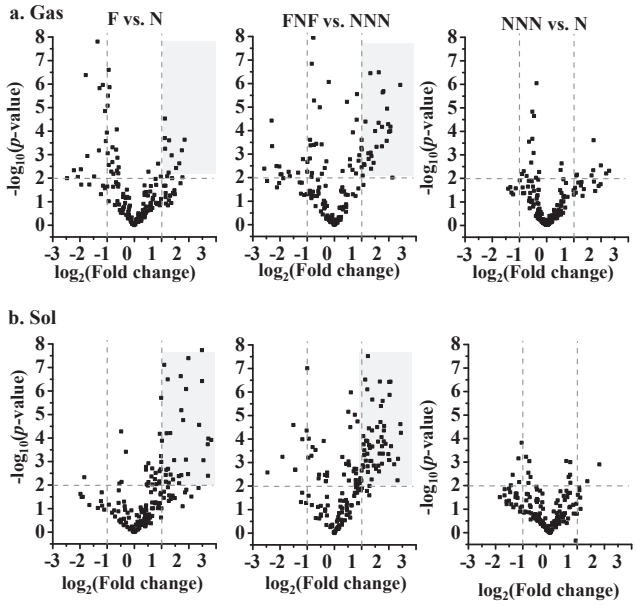

Fig. 1. Volcano plots showing the degree of the statistical *p*-value vs. fold change of 184 quantified lipid species in the groups of F (vs. N), FNF (vs. NNN), and NNN (vs. N). The horizontal dashed line represents the *p*-value of 0.01 and the two vertical dashed lines are borders for the 2-fold decrease and increase.

were quantified by SRM-based nUHPLC-ESI-MS/MS. The number of identified and quantified lipid species in each lipid class from skeletal muscles is listed in Table S4. The corrected peak area of each quantified lipid species from an individual animal in the six different diet groups is listed in Table S5. Lipid species of phosphatidylcholine (PC), phosphatidylethanolamine (PE), and TG were quantified by the total numbers of carbons and double bonds in the acyl chains, and the isomeric chain structures of each species were determined by collision-induced dissociation spectra (Table S6).

3.2. Overall change in lipid profile upon HFD

Variations in individual lipid levels of the Gas and Sol tissues under different HFD programs are represented using volcano plots, the plot of $-\log_{10}$ (*p*-value) vs. $\log_2$ (fold change) (Fig. 1), which depicts the overall changes in the F (vs. N) and FNF (vs. NNN) groups as well as a comparison of NNN with N group. Plots of the FNN and NNF groups are shown in Fig. S3. From the volcano plots, it is evident that lipid species with alterations after HFD treatment were mostly increased in the Sol, and the increase was > 2-fold in the F and FNF groups compared to that in the Gas. The changes in NNN and N were not significant except for a few species that showed an increase in the NNN group. This ascertains that lipid profiles in the two skeletal muscles at 8 weeks of age were not noticeably different. The overall differences in the lipid profiles of the Gas and Sol among the six different diet groups are illustrated using principal component analysis (PCA) (Fig. 2). The PCA plot showed that lipid profiles of the Sol in all groups were different from those of the Gas, and the data points of the Sol from mice after HFD treatment were clustered away from those from mice after normal diet treatment. This difference between the two diet groups of the Sol was relatively larger than that observed for the Gas. However, NNN and N groups of the Sol were in the same domain while those of the Gas were not. Figs. 1 and 2 show that lipid profiles of the Sol were more influenced by HFD than those of the Gas.

3.3. Change in lipid classes upon HFD

Changes in the composition of the lipids after HFD treatment can be

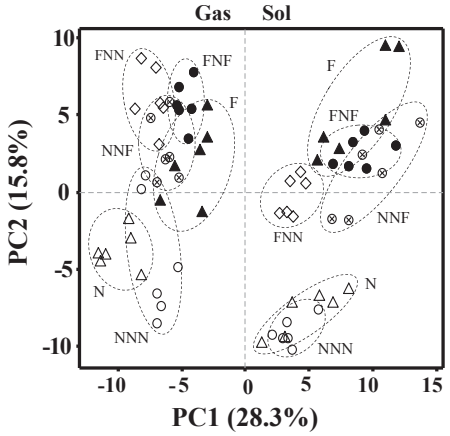

Fig. 2. Principal component analysis (PCA) showing the differences in lipid profiles of the Gas and Sol in mice under different diet programs (N, NNN, NNF, F, FNN, and FNF). Individual data points represent an individual animal.

viewed in the pie-charts (Fig. 3), depicting the relative occupancies (%) of the five abundant lipid classes in each group and "others" for the summed values for the remaining low abundance lipid classes. By comparing the total amount of lipids between the Gas and Sol, HFD appeared to significantly influence the Sol compared to the Gas. The total lipid content in the Gas did not show a significant elevation after the first 8 weeks of HFD treatment (1.09 for F vs. 1.00 for N), whereas in the Sol, the increase was ~35%. The last 4 weeks of HFD treatment resulted in 25% increase (NNF vs. NNN) in the Gas and 81% increase in the Sol. However, in the FNF group of both the Gas and Sol, ~50% increase was noted in comparison with the NNN groups. The mice subjected to the last 4 weeks of HFD treatment (FNF) compared to the FNN, both of which had HFD in the first 8 weeks, did not display a significant alteration in the lipid amounts in both the Gas (1.49 vs. 1.51 and Sol (1.55 vs. 1.40). Further, HFD altered the relative abundance of the lipid class. Especially, the relative abundance of PC (the most abundant class in N and NNN groups) decreased significantly and TG became the most abundant class of lipid after HFD treatment (F, NNF, FNN, and FNF). In the case of the Sol, TG remained the most abundant lipid class but the relative composition of PC decreased post-HFD due to the increase in PE, DG, and LPC. This can be associated with the enhanced accumulation of TG in the Gas compared to the Sol. However, the total amount of PC did not significantly alter upon HFD treatment as shown in the plot of fold change in Fig. 4a. HFD-induced changes in each lipid class can be viewed by plotting the fold changes in the four HFD groups (Fig. 4a) by comparing F with N and the other three (FNN, NNF, and FNF) groups relative to NNN. Corrected peak area of each lipid class in the six different mice groups are listed in Table S7. Fold changes of PC in the four groups were not significantly altered in all groups of Gas except F and in the Sol of F and FNF. Lipid profiles of NNN were not significantly different from N as shown in Fig. S4 except that LPC and DG increased by > 2.5-fold in the Gas while LPC did not change and DG increased by about 1.5 fold in Sol, HexCer was elevated by > 2-fold in the Sol, and both TG and Cer decreased by ~2-fold in the Sol. These can be considered as the alterations induced by aging under normal diet. As seen in Fig. 3, several lipid classes were elevated by HFD in the Sol compared to the Gas. While only PE and TG showed a significant ($p < 0.01$, > 2-fold) increase in the Gas of the FNN and FNF, most lipid classes were elevated in the Sol. Further, LPC, PI, and Cer in the Sol were significantly elevated in FNF. The PE and TG levels of the Gas were not significantly increased in NNF compared to FNN and FNF. This establishes the importance of the first 8 weeks of HFD on PE and TG in the Gas over the final 4 weeks of HFD. Nonetheless, a reverse trend was observed in the Sol. While the total PC level was not largely changed in the two tissues, PE levels significantly increased by

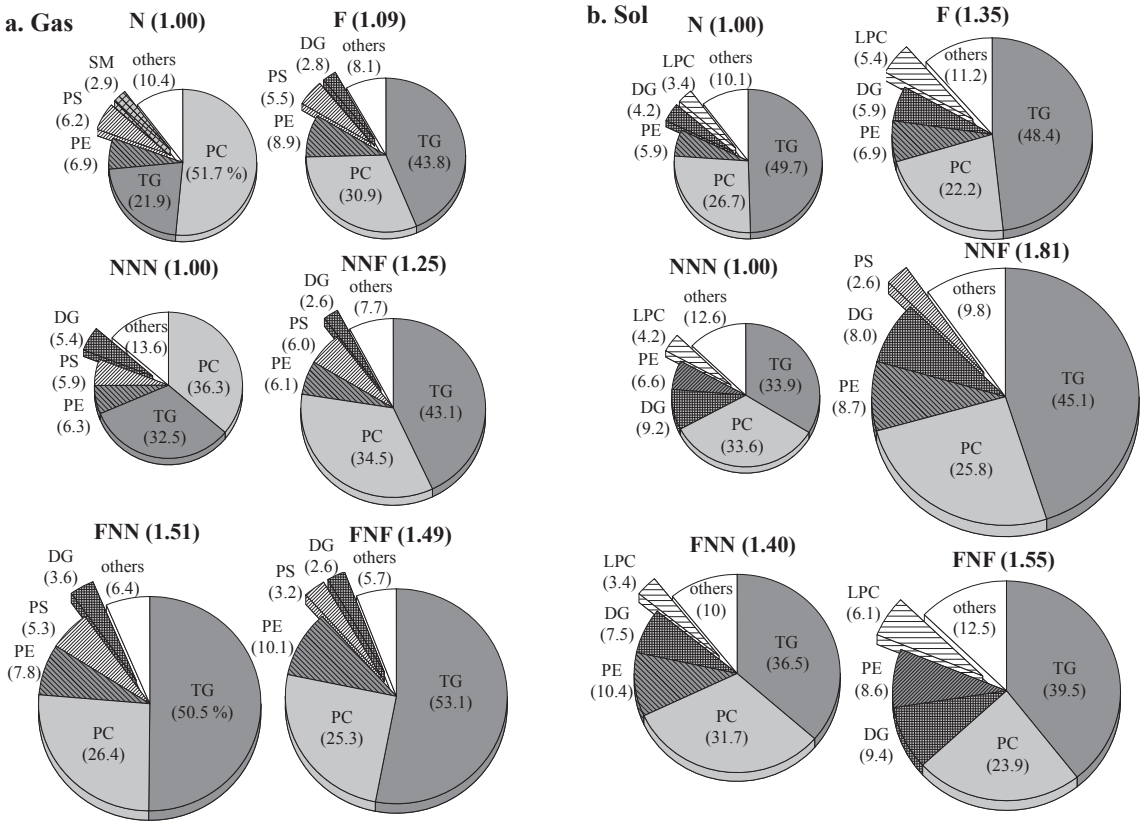

Fig. 3. Pie-charts showing the relative composition of lipid classes in the six diet groups (N, F, NNN, NNF, FNN, and FNF) in the a) Gas and b) Sol tissues. The amount of each lipid class was based on the corrected peak area (vs. IS of each class). Only the top five abundance lipid classes were plotted, and the remaining classes were represented as a summed amount marked with "others." The size of the pie-charts F is relative that of the N set as 1.00 and those of NNF, FNN and FNF are relative to those of the NNN group set as 1.00.

HFD treatment. PC/PE ratio (Fig. 4b) plotted for all six mice groups shows a large decrease in both the tissues of all HFD treated groups, except the Gas of the NNF group because the PE level in NNF did not change. The changes in the PC/PE ratio affect energy production by the mitochondria predominantly by changes in the PE levels. Energy storage molecules such as TG can accumulate with the increase in PE. In the case of NNF, a slight change in PE could be linked with the relatively low production of TG compared to that in the FNN and FNF groups (Fig. 4a). Taken together, the effect of HFD on the Gas in the first 8 weeks (FNN) appeared to be stronger than that in the final 4 weeks (NNF).

3.4. Lipid alterations at the molecular level

Alterations at the lipid molecular level are plotted using stacked bar graphs by representing the corrected peak area of each species between

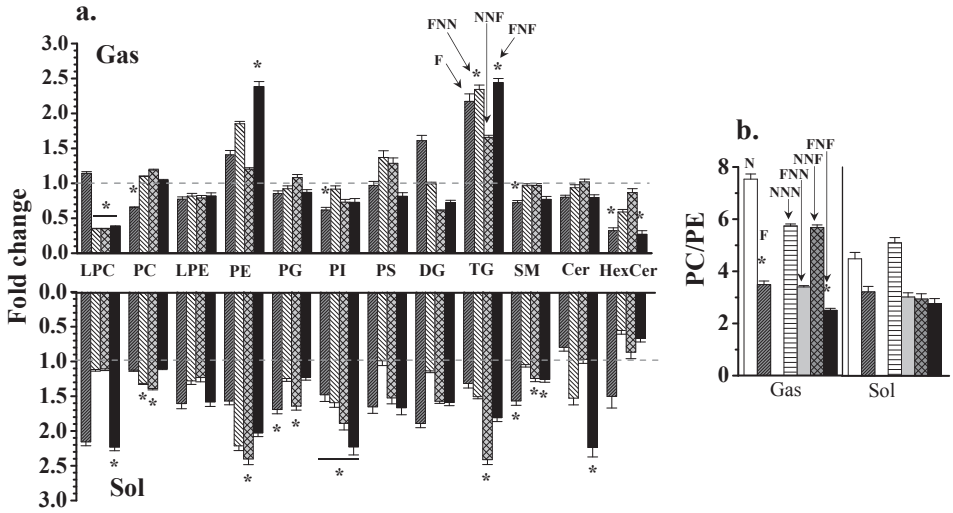

Fig. 4. Bar graphs representing the fold change (F vs. N and FNN, NNF, and FNF vs. NNN) at the lipid class level in the Gas and Sol. * for a significant difference with $p < 0.01$ and (b) PC/PE ratio in the Gas and Sol of all six mice groups.

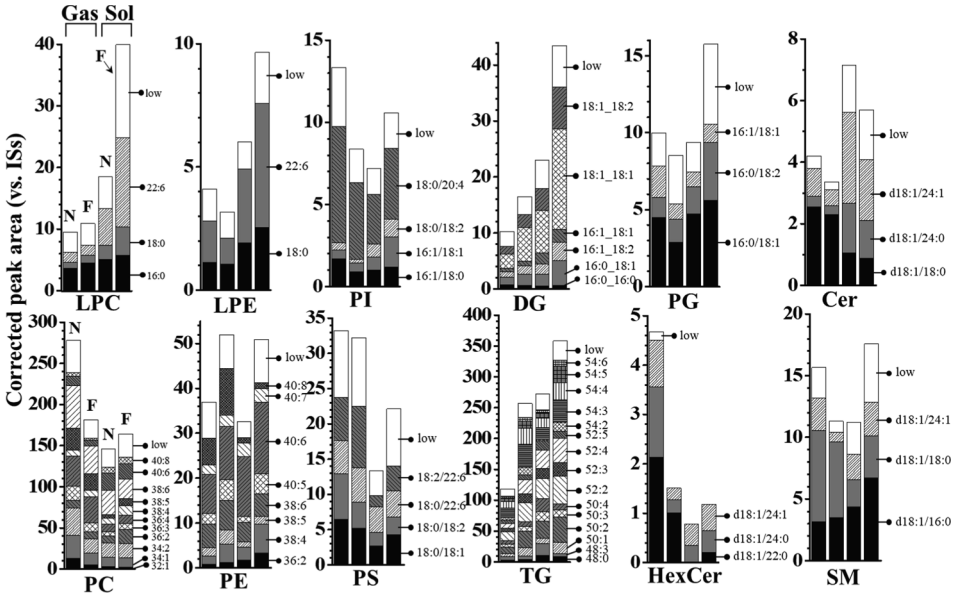

Fig. 5. Stacked bar graphs showing compositional differences in the corrected peak area (vs. IS) of each lipid class represented with the amount of individual lipid species in the N and F groups of the two muscular tissue types. The numbers (i.e. 16:0) at each bar represent the acyl chain structure of high abundance individual species. The "low" represents the summed amount of the low abundance species.

the Gas and Sol of the F and N groups (Fig. 5). High abundance species in each class were marked with acyl chain structures, and peak area of low abundance species was grouped into the white bar marked as "low." High abundance lipid is defined by its relative abundance > 100%/(total number of lipids within the class). After 8 weeks of HFD treatment, several TG in the Gas and the two LPC (18:0 and 22:6) with the five DG species in the Sol increased by ~2-fold. Further investigation on individual species was carried out to select lipids showing changes > 2-fold with $p < 0.01$ in comparison with the corresponding control group (N or NNN) and plotted using a heat map (Fig. S5). While most lipid species within the criteria appeared to increase with HFD in both the Gas and Sol, LPC decreased in the Gas but increased in the Sol. Further, TG species with relatively shorter acyl chain structure (48:3) decreased in both tissues but those with longer acyl chains mostly increased. HFD-induced alterations of the individual lipids were further investigated by the differences in HFD programs.

Fig. 6 further illustrates the significant fold change (vs. N or vs. NNN) of high abundance individual species from LPC, PI, DG, Cer, and TG classes (> 2-fold, $p < 0.01$). A significant decrease (> 2-fold) in LPC 16:0 and 18:0 in the Gas, which was known to be associated with inflammation, was observed in the FNN, NNF, and FNF groups, but LPC 18:0 and 22:6 in the Sol increased > 2-fold in the F and FNF groups. In the case of PI, which has an anti-inflammatory role, the two high abundant PI species (16:1/18:1 and 18:0/20:4) did not change in the Gas with HFD treatment. However, PI 16:1/18:1 increased by > 2-fold in the Sol of the F and FNF groups, and only PI 18:0/20:4 increased in the FNF group. Among the five DG species, two DG species (16:1_18:1 and 16:1_18:2) were down-regulated to a greater extent in the Gas than in the Sol, but the other three (16:0_18:1, 16:0_18:2, and 18:1_18:1) were up-regulated > 2-fold in the Sol. While the decrease in DG in the Gas was observed regardless of the HFD types, its increase in the Sol was less in the FNN group than in the other groups, suggesting that the accumulation of DG in the Sol is associated with the final 4 weeks of HFD treatment rather than the early stage treatments, which is in

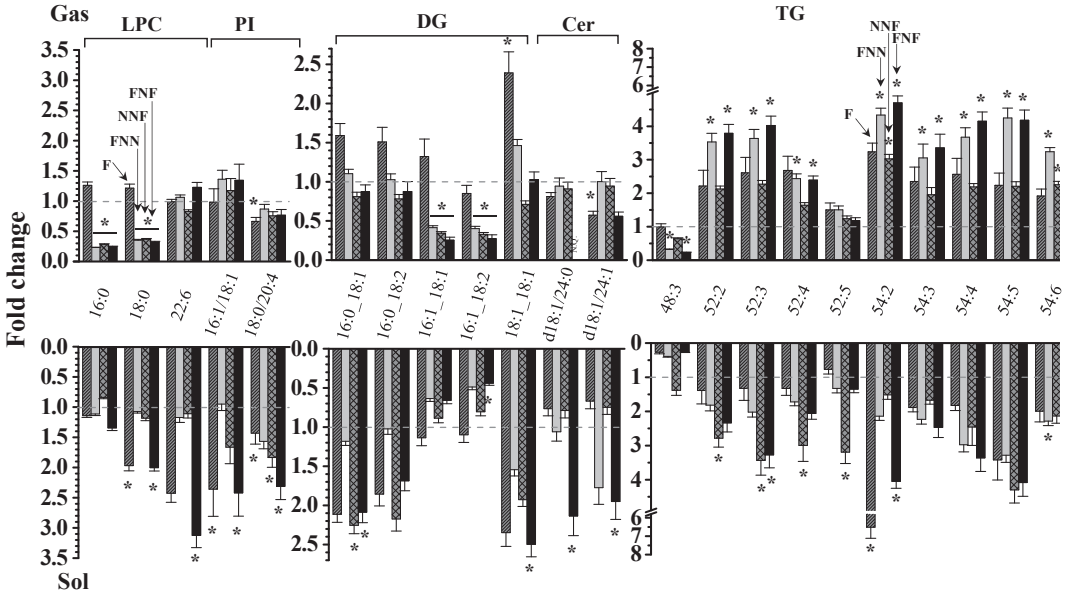

Fig. 6. Changes in the level of high abundance LPC, PI, DG, Cer, and TG species in the mice groups treated with different HFD programs: F (vs. N) and FNN, NNF, and FNF (vs. NNN). * for $p < 0.01$. The under-dash "_" in the acyl chain information of DG was used because the exact chain locations could not be completely resolved, while "/" was used for lipids when acyl chain locations at *sn*-1 and *sn*-2 can be differentiated by MS/MS spectra.

contrast to the observations with PE and TG in the Gas. Cer displayed a similar trend to DG, where Cer (d18:1/24:0 and d18:1/24:1) did not change or rather decreased in the Gas but significantly increased in the Sol of the FNF group. Most high abundance TG species significantly increased by 2–7 folds in both the Gas and Sol with HFD treatment, except the decrease of TG 48:3 (16:1/16:1/16:1 precisely) in the Gas. However, the accumulation of TG appeared to be higher in the Gas than in the Sol, and the patterns of increase were slightly different depending on the HFD program wherein most TG species in the Gas accumulated to a lesser extent in NNF than in FNN and FNF groups.

4. Discussion

LPC is known to be an important lipid effector of fatty acid-induced insulin resistance [43]. An earlier study revealed that increased LPC levels in cultured rat aortic vascular smooth muscle cells induced insulin resistance [44]. LPC has the role of inflammatory actions depending on its fatty acyl chain, and especially saturated LPC could act as pro-inflammatory mediators [45]. In this study, we observed that LPC 18:0 significantly accumulated in the Sol of the F and FNF groups while LPC 16:0 and 18:0 decreased in the Gas, indicating that HFD-induced increase of LPC was more effective in the Sol compared to the Gas of the FNF group. PI is known to exert an anti-inflammatory role by delivering arachidonic acid (20:4, AA), eicosanoids precursors that are inflammatory mediators [46,47]. An increased level of AA-containing PI might be an indicator of inflammation occurred in skeletal tissues [48]. Upon HFD treatment, muscle levels of high abundance PI (16:1/18:1 and 18:0/20:4) were not significantly altered in the Gas but increased substantially in the Sol of the F and FNF groups. Among these, a large increase in PI 18:0/20:4, the most abundant PI species in the Sol, might be related to the increased risk of inflammation. The abnormal ratio of PC/PE is reported to be detrimental for the membrane integrity and the energy-producing capability of mitochondria [49]. PE is the second most abundant phospholipid after PC in the mitochondria [50] and ATP levels are known to correlate with the PE levels [51]. A significant decrease in PC/PE of both the muscle tissues in most HFD groups was exclusively contributed by the elevated PE levels. This is consistent with the results of previous studies showing a reduction in PC/PE in the skeletal muscle due to increase in PE upon HFD treatment [52,53].

DG and Cer activate protein kinase C, thus, acting as mediators in the development of insulin resistance in the muscles [9]. Studies have shown that the levels of the four DG (16:0_18:1, 16:0_18:2, 18:0_18:1, and 18:1_18:1) in mouse skeletal muscles significantly ($>$ 2-fold, $p < 0.05$) increased after 16 weeks of HFD treatment, while Cer levels remained constant [3]. Recent studies have also revealed an increase in DG in the skeletal muscles upon HFD treatment and a negligible fold-change in Cer [53]. In this study, high abundance DG (16:0_18:1, 16:0_18:2, and 18:1_18:1) in the Sol of the F, NNF, and FNF groups were elevated $>$ 2-fold ($p < 0.01$). The two high abundance Cer (d18:1/24:0 and d18:1/24:1) were elevated $>$ 2-fold only in the Sol of the FNF group while they were not altered or rather decreased to some degree in the Gas. These results suggest that Sol is more responsive to HFD in terms of accumulating DG and Cer.

Excess TG accumulation in the muscles is generally considered as a signature for insulin resistance; however, trained endurance athletes can still maintain insulin sensitivity despite the increased intramuscular TG accumulation [13,14]. While several high abundance TG species in both the Gas and Sol (Fig. 6) displayed a significant increase, examining their detailed chain structures revealed that they are mostly mono-unsaturated acyl chains (Table S6c). Further, an overall increase in TG pattern appeared to be larger in the Gas of the FNN and FNF groups. This indicates that HFD in the first 8 weeks was critical for maintaining high levels of most TG species in the Gas because the levels of most TG in the Gas of NNF were lower than those of the FNN and FNF groups. However, Sol TG levels in the NNF group were rather inconsistent in the increasing patterns depending on the chain length, where TG with 52:x showed enhanced accumulation in the NNF but TG with 54:x did not.

Lastly, the different diet programs (weight maintenance, weight gain, and weight regain) did not affect most of the lipid profiles of the Gas except for PE and TG, which did not significantly change in the NNF. The results from the NNF group (fed with HFD in only the last 4 weeks) showed that the uptake of high-fat food in the younger age period appears to be more influential in the Gas than HFD uptake only in the later age period. However, Sol lipids altered by HFD treatment were more elevated by the weight regain program than other HFD programs, indicating that the Sol was more sensitive to HFD than was the Gas. Further studies are required to evaluate the effect of HFD on insulin resistance to elucidate the relationship between muscle and circulating lipids.

CRediT authorship contribution statement

Jung Yong Eum: Formal analysis, Data curation. **Gwang Bin Lee:** Formal analysis. **Sun Shin Yi:** Investigation. **Il Yong Kim:** Investigation. **Je Kyung Seong:** Validation. **Myeong Hee Moon:** Writing - original draft, Supervision.

Declaration of Competing Interest

The authors declare that they have no known competing financial interests or personal relationships that could have appeared to influence the work reported in this paper.

Acknowledgements

This study was supported by the grant (NRF-2018R1A2A1A05019794) and in part by Korea Mouse Phenotyping project (NRF-2017M3A9D5A01052447) of the Ministry of Science, ICT & Future Planning through the National Research Foundation (NRF) of Korea. Mouse samples were provided by the Korea Mouse Phenotyping Center.

Declaration of Competing Interest

The authors declare that they have no conflict of interest.

Appendix A. Supplementary material

Supplementary data to this article can be found online at https://doi.org/10.1016/j.jchromb.2020.122022.

References

[1] R.H. Eckel, S.M. Grundy, P.Z. Zimmet, The metabolic syndrome, Lancet 365 (2005) 1415–1428.
[2] B.H. Goodpaster, D. Wolf, Skeletal muscle lipid accumulation in obesity, insulin resistance, and type 2 diabetes, Pediatr. Diabetes 5 (2004) 219–226.
[3] N. Turner, G.M. Kowalski, S.J. Leslie, S. Risis, C. Yang, R.S. Lee-Young, J.R. Babb, P.J. Meikle, G.I. Lancaster, D.C. Henstridge, P.J. White, E.W. Kraegen, A. Marette, G.J. Cooney, M.A. Febbraio, C.R. Bruce, Distinct patterns of tissue-specific lipid accumulation during the induction of insulin resistance in mice by high-fat feeding, Diabetologia 56 (2013) 1638–1648.
[4] M.R. Wenk, The emerging field of lipidomics, Nat. Rev. Drug. Discov. 4 (2005) 594–610.
[5] A. Bosio, E. Binczek, W. Stoffel, Functional breakdown of the lipid bilayer of the myelin membrane in central and peripheral nervous system by disrupted galactocerebroside synthesis, Proc. Natl. Acad. Sci. U. S. A. 93 (1996) 13280–13285.
[6] K.T. Tonks, A.C. Coster, M.J. Christopher, R. Chaudhuri, A. Xu, J. Gagnon-Bartsch, D.J. Chisholm, D.E. James, P.J. Meikle, J.R. Greenfield, D. Samocha-Bonet, Skeletal muscle and plasma lipidomic signatures of insulin resistance and overweight/obesity in humans, Obesity (Silver Spring) 24 (2016) 908–916.
[7] Y.K. Magnusson, P. Friberg, P. Sjovall, J. Malm, Y. Chen, TOF-SIMS analysis of lipid accumulation in the skeletal muscle of ob/ob mice, Obesity (Silver Spring) 16 (2008) 2745–2753.
[8] G.I. Shulman, Cellular mechanisms of insulin resistance, J. Clin. Invest. 106 (2000) 171–176.

[9] B.D. Hegarty, S.M. Furler, J. Ye, G.J. Cooney, E.W. Kraegen, The role of intramuscular lipid in insulin resistance, Acta Physiol. Scand. 178 (2003) 373–383.
[10] N.G. Forouhi, G. Jenkinson, E.L. Thomas, S. Mullick, S. Mierisova, U. Bhonsle, P.M. McKeigue, J.D. Bell, Relation of triglyceride stores in skeletal muscle cells to central obesity and insulin sensitivity in European and South Asian men, Diabetologia 42 (1999) 932–935.
[11] B.H. Goodpaster, F.L. Thaete, J.A. Simoneau, D.E. Kelley, Subcutaneous abdominal fat and thigh muscle composition predict insulin sensitivity independently of visceral fat, Diabetes 46 (1997) 1579–1585.
[12] N.D. Oakes, S. Camilleri, S.M. Furler, D.J. Chisholm, E.W. Kraegen, The insulin sensitizer, BRL 49653, reduces systemic fatty acid supply and utilization and tissue lipid availability in the rat, Metabolism 46 (1997) 935–942.
[13] B.H. Goodpaster, J. He, S. Watkins, D.E. Kelley, Skeletal muscle lipid content and insulin resistance: evidence for a paradox in endurance-trained athletes, J. Clin. Endocrinol. Metab. 86 (2001) 5755–5761.
[14] F. Amati, J.J. Dube, E. Alvarez-Carnero, M.M. Edreira, P. Chomentowski, P.M. Coen, G.E. Switzer, P.E. Bickel, M. Stefanovic-Racic, F.G. Toledo, B.H. Goodpaster, Skeletal muscle triglycerides, diacylglycerols, and ceramides in insulin resistance: another paradox in endurance-trained athletes? Diabetes 60 (2011) 2588–2597.
[15] A. Kotronen, V.R. Velagapudi, L. Yetukuri, J. Westerbacka, R. Bergholm, K. Ekroos, J. Makkonen, M.R. Taskinen, M. Oresic, H. Yki-Jarvinen, Serum saturated fatty acids containing triacylglycerols are better markers of insulin resistance than total serum triacylglycerol concentrations, Diabetologia 52 (2009) 684–690.
[16] V.T. Samuel, K.F. Petersen, G.I. Shulman, Lipid-induced insulin resistance: unravelling the mechanism, Lancet 375 (2010) 2267–2277.
[17] S.I. Itani, N.B. Ruderman, F. Schmieder, G. Boden, Lipid-induced insulin resistance in human muscle is associated with changes in diacylglycerol, protein kinase C, and IkappaB-alpha, Diabetes 51 (2002) 2005–2011.
[18] D.M. Erion, G.I. Shulman, Diacylglycerol-mediated insulin resistance, Nat. Med. 16 (2010) 400–402.
[19] M. Gueugneau, C. Coudy-Gandilhon, L. Theron, B. Meunier, C. Barboiron, L. Combaret, D. Taillandier, C. Polge, D. Attaix, B. Picard, J. Verney, F. Roche, L. Feasson, J.C. Barthelemy, D. Bechet, Skeletal muscle lipid content and oxidative activity in relation to muscle fiber type in aging and metabolic syndrome, J. Gerontol. A. Biol. Sci. Med. Sci. 70 (2015) 566–576.
[20] C. Hidalgo, G. Sanchez, G. Barrientos, P. Aracena-Parks, A transverse tubule NADPH oxidase activity stimulates calcium release from isolated triads via ryanodine receptor type 1 S -glutathionylation, J. Biol. Chem. 281 (2006) 26473–26482.
[21] D.B. Savage, K.F. Petersen, G.I. Shulman, Disordered lipid metabolism and the pathogenesis of insulin resistance, Physiol. Rev. 87 (2007) 507–520.
[22] R. Liu, P. Jin, L. Yu, Y. Wang, L. Han, T. Shi, X. Li, Impaired mitochondrial dynamics and bioenergetics in diabetic skeletal muscle, PLoS ONE 9 (2014) e92810.
[23] D. Xu, Z. Jiang, Z. Sun, L. Wang, G. Zhao, H.M. Hassan, S. Fan, W. Zhou, S. Han, L. Zhang, T. Wang, Mitochondrial dysfunction and inhibition of myoblast differentiation in mice with high-fat-diet-induced pre-diabetes, J. Cell. Physiol. 234 (2019) 7510–7523.
[24] J.R. Zierath, J.A. Hawley, Skeletal muscle fiber type: influence on contractile and metabolic properties, PLoS Biol. 2 (2004) e348.
[25] A.C. Loureiro, I.C. do Rego-Monteiro, R.A. Louzada, V.H. Ortenzi, A.P. de Aguiar, E.S. de Abreu, J.P. Cavalcanti-de-Albuquerque, F. Hecht, A.C. de Oliveira, V.M. Ceccatto, R.S. Fortunato, D.P. Carvalho, Differential expression of NADPH oxidases depends on skeletal muscle fiber type in rats, Oxid. Med. Cell Longev. 2016 (2016) 6738701.
[26] M. Picard, R.T. Hepple, Y. Burelle, Mitochondrial functional specialization in glycolytic and oxidative muscle fibers: tailoring the organelle for optimal function, Am. J. Physiol. Cell. Physiol. 302 (2012) C629–C641.
[27] M.C. Levin, M. Monetti, M.J. Watt, M.P. Sajan, R.D. Stevens, J.R. Bain, C.B. Newgard, R.V. Farese Sr., R.V. Farese Jr., Increased lipid accumulation and insulin resistance in transgenic mice expressing DGAT2 in glycolytic (type II) muscle, Am. J. Physiol. Endocrinol. Metab 293 (2007) E1772–E1781.
[28] J.C. Lee, I.Y. Kim, Y. Son, S.K. Byeon, D.H. Yoon, J.S. Son, H.S. Song, W. Song, J.K. Seong, M.H. Moon, Evaluation of treadmill exercise effect on muscular lipid profiles of diabetic fatty rats by nanoflow liquid chromatography-tandem mass spectrometry, Sci. Rep. 6 (2016) 29617.
[29] C.N. Lumeng, J.L. Bodzin, A.R. Saltiel, Obesity induces a phenotypic switch in adipose tissue macrophage polarization, J. Clin. Investig. 117 (2007) 175–184.
[30] F.L. Greenway, Physiological adaptations to weight loss and factors favouring weight regain, Int. J. Obesity 39 (2015) 1188–1196.
[31] R. Taguchi, J. Hayakawa, Y. Takeuchi, M. Ishida, Two-dimensional analysis of phospholipids by capillary liquid chromatography/electrospray ionization mass spectrometry, J. Mass. Spectrom. 35 (2000) 953–966.
[32] R. Taguchi, T. Houjou, H. Nakanishi, T. Yamazaki, M. Ishida, M. Imagawa, T. Shimizu, Focused lipidomics by tandem mass spectrometry, J. Chromatogr. B. Analyt. Technol. Biomed. Life. Sci. 823 (2005) 26–36.
[33] D.Y. Bang, M.H. Moon, On-line two-dimensional capillary strong anion exchange/reversed phase liquid chromatography-tandem mass spectrometry for comprehensive lipid analysis, J. Chromatogr. A 1310 (2013) 82–90.
[34] S.K. Byeon, J.Y. Lee, S. Lim, D. Choi, M.H. Moon, Discovery of candidate phospholipid biomarkers in human lipoproteins with coronary artery disease by flow field-flow fractionation and nanoflow liquid chromatography-tandem mass spectrometry, J. Chromatogr. A 1270 (2012) 246–253.
[35] P.D. Rainville, C.L. Stumpf, J.P. Shockcor, R.S. Plumb, J.K. Nicholson, Novel application of reversed-phase UPLC-oaTOF-MS for lipid analysis in complex biological mixtures: a new tool for lipidomics, J. Proteome. Res. 6 (2007) 552–558.
[36] S.K. Byeon, J.C. Lee, B.C. Chung, H.S. Seo, M.H. Moon, High-throughput and rapid quantification of lipids by nanoflow UPLC-ESI-MS/MS: application to the hepatic lipids of rabbits with nonalcoholic fatty liver disease, Anal. Bioanal. Chem. 408 (2016) 4975–4985.
[37] J.C. Lee, S.K. Byeon, M.H. Moon, Relative quantification of phospholipids based on isotope-labeled methylation by nanoflow ultrahigh performance liquid chromatography-tandem mass spectrometry: enhancement in cardiolipin profiling, Anal. Chem. 89 (2017) 4969–4977.
[38] J.C. Lee, S.M. Park, I.Y. Kim, H. Sung, J.K. Seong, M.H. Moon, High-fat diet-induced lipidome perturbations in the cortex, hippocampus, hypothalamus, and olfactory bulb of mice, Biochim. Biophys. Acta, Lipids. Lipid. Metab. 2018 (1863) 980–990.
[39] S.K. Byeon, J.Y. Lee, M.H. Moon, Optimized extraction of phospholipids and lysophospholipids for nanoflow liquid chromatography-electrospray ionization-tandem mass spectrometry, Analyst 137 (2012) 451–458.
[40] S. Lim, S.K. Byeon, J.Y. Lee, M.H. Moon, Computational approach to structural identification of phospholipids using raw mass spectra from nanoflow liquid chromatography-electrospray ionization-tandem mass spectrometry, J. Mass. Spectrom. 47 (2012) 1004–1014.
[41] K. Yang, X. Han, Accurate quantification of lipid species by electrospray ionization mass spectrometry - Meet a key challenge in lipidomics, Metabolites 1 (2011) 21–40.
[42] J. Wang, C. Wang, X. Han, Tutorial on lipidomics, Anal. Chim. Acta 1061 (2019) 28–41.
[43] M.S. Han, Y.M. Lim, W. Quan, J.R. Kim, K.W. Chung, M. Kang, S. Kim, S.Y. Park, J.S. Han, S.Y. Park, H.G. Cheon, S. Dal Rhee, T.S. Park, M.S. Lee, Lysophosphatidylcholine as an effector of fatty acid-induced insulin resistance, J. Lipid. Res. 52 (2011) 1234–1246.
[44] E.D. Motley, S.M. Kabir, C.D. Gardner, K. Eguchi, G.D. Frank, T. Kuroki, M. Ohba, T. Yamakawa, S. Eguchi, Lysophosphatidylcholine inhibits insulin-induced Akt activation through protein kinase C-alpha in vascular smooth muscle cells, Hypertension 39 (2002) 508–512.
[45] J.M. Del Bas, A. Caimari, M.I. Rodriguez-Naranjo, C.E. Childs, C. Paras Chavez, A.L. West, E.A. Miles, L. Arola, P.C. Calder, Impairment of lysophospholipid metabolism in obesity: altered plasma profile and desensitization to the modulatory properties of n-3 polyunsaturated fatty acids in a randomized controlled trial, Am. J. Clin. Nutr. 104 (2016) 266–279.
[46] A.M. Lone, K. Tasken, Proinflammatory and immunoregulatory roles of eicosanoids in T cells, Front. Immunol. 4 (2013) 130.
[47] J.M. van Dieren, Y. Simons-Oosterhuis, H.C. Raatgeep, D.J. Lindenbergh-Kortleve, M.E. Lambers, C.J. van der Woude, E.J. Kuipers, G.T. Snoek, R. Potman, H. Hammad, B.N. Lambrecht, J.N. Samsom, E.E. Nieuwenhuis, Anti-inflammatory actions of phosphatidylinositol, Eur. J. Immunol. 41 (2011) 1047–1057.
[48] N. Goto-Inoue, K. Yamada, A. Inagaki, Y. Furuichi, S. Ogino, Y. Manabe, M. Setou, N.L. Fujii, Lipidomics analysis revealed the phospholipid compositional changes in muscle by chronic exercise and high-fat diet, Sci. Rep. 3 (2013) 3267.
[49] Z. Li, L.B. Agellon, T.M. Allen, M. Umeda, L. Jewell, A. Mason, D.E. Vance, The ratio of phosphatidylcholine to phosphatidylethanolamine influences membrane integrity and steatohepatitis, Cell. Metab. 3 (2006) 321–331.
[50] G. Tasseva, H.D. Bai, M. Davidescu, A. Haromy, E. Michelakis, J.E. Vance, Phosphatidylethanolamine deficiency in Mammalian mitochondria impairs oxidative phosphorylation and alters mitochondrial morphology, J. Biol. Chem. 288 (2013) 4158–4173.
[51] J.N. van der Veen, S. Lingrell, R.P. da Silva, R.L. Jacobs, D.E. Vance, The concentration of phosphatidylethanolamine in mitochondria can modulate ATP production and glucose metabolism in mice, Diabetes 63 (2014) 2620–2630.
[52] M.K. Montgomery, S.H.J. Brown, T.W. Mitchell, A.C.F. Coster, G.J. Cooney, N. Turner, Association of muscle lipidomic profile with high-fat diet-induced insulin resistance across five mouse strains, Sci. Rep. 7 (2017) 13914.
[53] A.B. Jordy, M.J. Kraakman, T. Gardner, E. Estevez, H.L. Kammoun, J.M. Weir, B. Kiens, P.J. Meikle, M.A. Febbraio, D.C. Henstridge, Analysis of the liver lipidome reveals insights into the protective effect of exercise on high-fat diet-induced hepatosteatosis in mice, Am. J. Physiol. Endocrinol. Metab 308 (2015) E778–E791.